

Thin-film flooded agglomerate model for silver-based oxygen depolarized cathodes

Stefan Pinnow · Naresh Chavan · Thomas Turek

Received: 9 December 2010 / Accepted: 7 April 2011 / Published online: 18 May 2011
© Springer Science+Business Media B.V. 2011

Abstract A mathematical model for a porous, silver-based electrode for the oxygen reduction in alkaline solutions, based on the thin film flooded agglomerate theory, was developed. These electrodes are employed in the energy-efficient chlor-alkali electrolysis with oxygen depolarized cathodes. The model parameters were determined from overpotentials at different oxygen concentrations obtained in half-cell measurements. For the description of the reaction kinetics, it was necessary to introduce two Tafel equations, which might be explained by a change of the adsorption isotherm of the intermediate species during oxygen reduction. The model allows for a successful description of the overpotentials in the region of industrially relevant current densities. The analysis of the oxygen concentration distribution in the liquid electrolyte reveals that massive diffusion limitations occur although the calculated size of the agglomerates is only in the range of a few micrometers.

Keywords Oxygen reduction · Ag · Chlor-alkali electrolysis · Modeling

List of symbols

A	Constant describing the exchange current density (A m mol^{-1})
c	Molar concentration of oxygen dissolved in NaOH solution at boundary film–agglomerate (mol m^{-3})
c^*	Molar concentration of oxygen dissolved in NaOH solution at boundary gas–film (mol m^{-3})

c_i	Molar concentration of species i (mol m^{-3})
D_{ij}	Binary Maxwell–Stefan diffusion coefficient for species i and j ($\text{m}^2 \text{s}^{-1}$)
$D_{i,K}$	Knudsen diffusion coefficient for species i ($\text{m}^2 \text{s}^{-1}$)
E°	Equilibrium potential (V)
E_{change}	Potential of change in Tafel slope (V)
F	Faraday constant ($= 96485.3399(24) \text{ C mol}^{-1}$)
H	Henry constant ($\text{Pa m}^3 \text{mol}^{-1}$)
j	Current density (A m^{-2})
k_c	(Chemical) reaction rate constant (s^{-1})
L	Characteristic length (m)
m	Molality of NaOH solution (mol kg^{-1})
M_i	Molar mass of species i (kg mol^{-1})
N_i	Flux of species i ($\text{mol m}^{-2} \text{s}^{-1}$)
P_i	Partial pressure of species i (Pa)
P_m	Saturation partial pressure of water above NaOH solution (Pa)
R	Universal gas constant ($= 8.314472(15) \text{ J mol}^{-1} \text{ K}^{-1}$)
r	Radius (m)
r_{ag}	Radius of agglomerates (m)
r	Reaction rate ($\text{mol m}^{-3} \text{s}^{-1}$)
S_{tf}	Specific surface area of thin film per total volume of reaction layer ($\text{m}^2 \text{m}^{-3}$)
T_s	Tafel slope (V decade $^{-1}$)
T	Temperature (K)
z	Length domain in reaction layer (m)
z'	Length domain in gas diffusion layer (m)
z''	Length domain in boundary layer (m)

Greek letters

δ_{tf}	Thickness of thin film (m)
$\Delta\varphi$	Potential difference between solid electrode and electrolyte (V)
ε	Porosity (dimensionless)

S. Pinnow · N. Chavan · T. Turek (✉)
Institute of Chemical Process Engineering, TU Clausthal
Leibnizstr. 17, 38678 Clausthal-Zellerfeld, Germany
e-mail: turek@icvt.tu-clausthal.de

γ_{\pm}	Mean molal activity coefficient of NaOH solution (dimensionless)
γ	Thiele modulus (dimensionless)
η_{eff}	Effectiveness factor (dimensionless)
η	Overpotential (V)
κ	Electronic/ionic conductivity (S m^{-1})
μ_i	Chemical potential of species i (J mol^{-1})
π	$= 3.14159265\dots$
ρ_{NaOH}	Density of NaOH solution (kg m^{-3})
τ	Tortuosity (dimensionless)
φ	Potential (V)

Subscripts

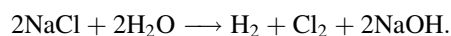
b	Boundary layer
e	Electronic, solid phase of agglomerates
g	Gas chamber
i	Ionic, liquid phase of agglomerates
n	Agglomerate phase in reaction layer
s	Gas diffusion layer
T	Total
t	Gas phase in reaction layer
tf	Thin film
H_2O	Total water (gaseous + liquid)

Superscripts

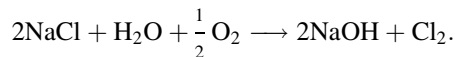
\ominus	Standard state
eff	Effective
g	Gas phase
l	Liquid phase

1 Introduction

Silver is an excellent catalyst for the oxygen reduction in alkaline solutions and silver-based gas diffusion electrodes or oxygen depolarized cathodes (ODCs) are used in alkaline fuel cells, metal-air batteries, and advanced chlor-alkali electrolysis processes. Especially the latter application has attracted considerable interest since chlor-alkali electrolysis—one of the most important chemical processes with a world chlorine capacity of 62.8 million metric tons in 2008 [1]—has a very high energy demand. In the classical process, chlorine, hydrogen, and sodium hydroxide are produced from an aqueous sodium chloride solution according to the following stoichiometry



In cases where the byproduct hydrogen cannot be used for chemical syntheses, the replacement of the standard hydrogen evolving cathodes by an ODC allows for a cell voltage reduction of about 1 V equivalent to 30% of the electrical energy demand [2]. The overall reaction of this modified process is



With currently available ODCs, the operation of the electrolysis process at industrial current densities is only possible with pure oxygen, the cost of which reduces the overall economic advantage. However, it could be shown in a recent study that even at present electricity prices the application of ODCs in chlor-alkali electrolysis cells is profitable [3]. Bayer MaterialScience AG have announced that a first commercial plant using this new technology with an annual chlorine capacity of 20 kt will go on stream in 2011 [4].

For the further improvement of ODCs, it is highly desirable to develop a mathematical model including the relevant structural and physico-chemical properties of the electrode and the reactants, i.e., oxygen and water in the concentrated sodium hydroxide solution. To our knowledge, only the papers of Wang and Koda deal with the performance of an oxygen depolarized cathode in a chlor-alkali electrolysis cell [5, 6]. However, several other models for the description of cathodes in alkaline fuel cells have been developed [7]. These electrodes have many similarities to ODCs used for the chlor-alkali electrolysis. The first developed models were based on a simple pore and thin-film approach proposed by Austin and Will [8, 9] and extended by Srinivasan [10, 11]. At the same time, dual scale porosity models were used by Markin and Busstein [12, 13]. Grens proposed the flooded porous electrode model [14, 15]. Finally, the flooded agglomerate model from Giner [16] was extended by Cutlip to the so-called thin-film flooded agglomerate (TFFA) model [17] which was used in further study by Iczkowski, Björnbom, and Yang [18–21]. This model can be regarded as current state-of-the-art in fuel cell electrode modeling and was also used by Wang and Koda [6] in their study.

In this article, we extended the model of Wang and Koda taking additionally into account the presence of other gases than oxygen (nitrogen and water vapor) as well as a refined description of the electrolyte using the concentrated electrolyte theory from Newman [22, 23]. We then determined reaction rate constants and the geometrical model parameters by comparison with measured overpotentials as a function of current density during oxygen reduction. The most important limitations of the oxygen reduction in ODCs and possible ways for improving the electrode performance will be discussed.

2 Model assumptions

The model describes a porous oxygen depolarized cathode in contact with the liquid electrolyte on the one hand side

and gas on the other hand side (Fig. 1). Electrolyte and gas are in intimate contact in the reaction layer whereas the gaseous reactant is transported from the gas chamber through a stagnant boundary layer and the part of the electrode that is not filled with electrolyte (gas diffusion layer). A comparison of typical geometrical model assumptions with a real silver-based oxygen depolarized cathode prepared by a spray method is shown in Fig. 2. The left hand side of the figure shows a macroscopic view of the porous structure with a thickness of less than 1 mm placed on a metal net as current collector. On the right hand side, one can see the assumed sizes of liquid and gas filled regions as well as the real pore structure formed by Ag particles and PTFE fibers. The model assumptions are as follows:

1. The electrode is operated in steady state at constant temperature.
2. The total pressure is constant in all regions.
3. The gas diffusion layer has a length z_s and consists of gas filled pores which can be characterized with the average pore radius r_s , the porosity ε_s and the tortuosity τ_s .
4. The reaction layer has the length z_t and consists of gas pores and agglomerates which are filled with electrolyte and surrounded by a thin liquid film.
5. The gas pores in the reaction layer are of cylindrical shape and have a uniform radius of r_t . The volume fraction of the gas channels in the reaction layer corresponds to the porosity ε_t . The tortuosity of the gas channels τ_t is 1 due to the cylindrical shape.
6. The “flooded agglomerates” consisting of the solid electrode and the liquid electrolyte are also of cylindrical shape and have a uniform radius r_{ag} , a porosity ε_n , and a tortuosity τ_n .
7. The thin film which surrounds the agglomerates has a very small thickness δ_{tf} , thus the surface of the agglomerates related to the volume of the reaction layer S_{tf} can be calculated with r_{ag} .
8. The considered gaseous species in the diffusion and reaction layer are oxygen, water vapor, and nitrogen. Both, the free and the Knudsen diffusion are considered. Since there may be more than two species present, the Maxwell–Stefan diffusion equations are used.
9. Between the porous ODC and the gas chamber, we assume a stagnant film with a thickness z_b . The diffusion through the film is modeled with the Maxwell–Stefan equations.
10. At the surface between the gas channels and the liquid film, the oxygen dissolves in the electrolyte and then diffuses perpendicular to the axis of the agglomerate. It is assumed that the electrolyte is in

equilibrium with the oxygen in the gas phase and that Henry's law is applicable. Since the dissolution of nitrogen in the electrolyte is neglected, it is sufficient to describe the diffusion of oxygen in the film and the agglomerate by Fick's law.

11. Water is allowed to change between the gas phase and the liquid phase and equilibrium is assumed between these phases.
 12. In the liquid phase, the species water, sodium ions, hydroxide ions, and dissolved oxygen are assumed to be present. As oxygen is only flowing perpendicular to the other species, it is not considered in the direction along the agglomerate. The other three species are modeled with the Maxwell–Stefan equations.
 13. The electrochemical reaction considered is the direct four electron reaction of oxygen and water
- $$\text{O}_2 + 2\text{H}_2\text{O} + 4e^- \longrightarrow 4\text{OH}^- \quad (1)$$
- The possible formation of hydrogen peroxide as intermediate is neglected because silver has a very high catalytic activity for peroxide decomposition. However, it is necessary to take into account a change of the rate determining step in the overall reaction at a certain potential E_{change} . This assumption will be discussed in more detail later.
14. The electrochemical reaction is assumed to be first order in the oxygen concentration.

3 Model equations

In this section the model equations for the various regions (cf. Fig. 1) are summarized. For further illustration Fig. 3 shows all possible flow directions of the chemical species and the current.

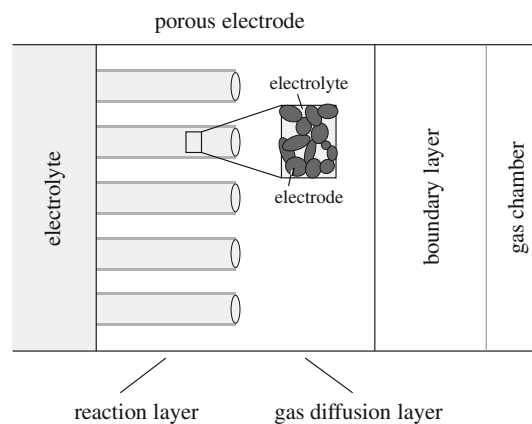


Fig. 1 Assumed geometry of the model

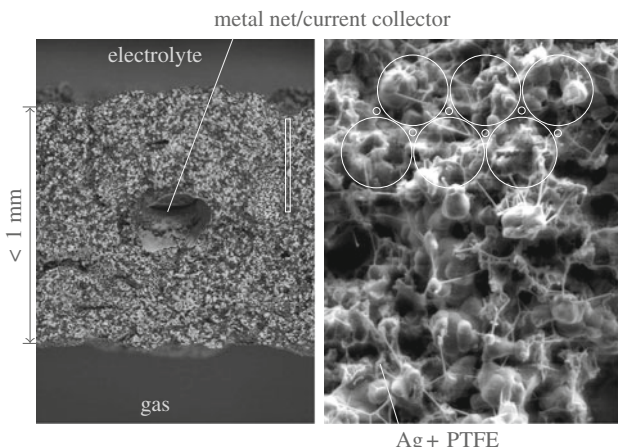


Fig. 2 Structure of a silver-based oxygen depolarized cathode

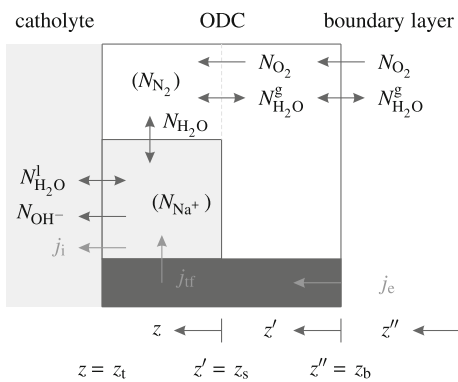


Fig. 3 Possible flow directions of chemical species and current

3.1 Boundary layer in the gas chamber

The diffusion of the gases through the boundary layer between the well-mixed part of the gas chamber and the diffusion layer in the ODC is described with the Maxwell–Stefan equations.

$$-\frac{1}{RT} \frac{dP_i}{dz''} = \sum_{j=1}^n \frac{P_j N_i - P_i N_j}{P_{T,b} D_{ij}^g} \quad (2)$$

3.2 Gas diffusion in the ODC

In contrast to Eq. 2, the diffusion is now taking place in a porous medium and thus the effective values of diffusion coefficients $D_{ij,s}^{\text{eff}}$ and Knudsen diffusion coefficients $D_{i,K,s}^{\text{eff}}$ have to be considered.

$$-\frac{1}{RT} \frac{dP_i}{dz'} = \frac{N_i}{D_{i,K,s}^{\text{eff}}} + \sum_{j=1}^n \frac{P_j N_i - P_i N_j}{P_{T,s} D_{ij,s}^{\text{eff}}} \quad (3)$$

$$-\frac{1}{RT} \frac{dP_i}{dz} = \frac{N_i}{D_{i,K,t}^{\text{eff}}} + \sum_{\substack{j=1 \\ j \neq i}}^n \frac{P_j N_i - P_i N_j}{P_{T,t} D_{ij,t}^{\text{eff}}} \quad (4)$$

3.3 Electrolyte diffusion

Since a strong electrolyte consisting of the ions Na^+ and OH^- in H_2O at high concentrations is considered, one must account for the real behavior of the ions. This can be achieved by using the chemical potential μ_i of the different species.

$$-\frac{c_i}{RT} \frac{d\mu_i}{dz} = \sum_{\substack{j=1 \\ j \neq i}}^n \frac{c_j N_i - c_i N_j}{c_T D_{ij,n}^{\text{eff}}} \quad (5)$$

With the aid of the electroneutrality law and the definition of the mean molal activity coefficient γ_{\pm} , one obtains

$$\begin{aligned} \mu_{\text{NaOH}} &= \mu_{\text{Na}^+} + \mu_{\text{OH}^-} \\ &= \mu_{\text{NaOH}}^\phi + RT \ln(\gamma_{\pm}^2 m^2). \end{aligned} \quad (6)$$

Thus, it is sufficient to calculate the change of the molality m as a function of z .

$$\frac{dm}{dz} = \frac{m}{2RT} \cdot \frac{\frac{d\mu_{\text{NaOH}}}{dz}}{1 + m \ln 10 \frac{d \log \gamma_{\pm}}{dm}} \quad (7)$$

The change of γ_{\pm} with respect to z can be calculated with the extended Debye–Hückel limiting law for strong electrolytes [24].

$$\log \gamma_{\pm} = \frac{-u\sqrt{m}}{1 + \sqrt{2m}} + Bm + Cm^2 + Dm^3 + Em^4$$

The derivative with respect to the molality gives

$$\begin{aligned} \frac{d \log \gamma_{\pm}}{dm} &= \frac{-u\sqrt{2}}{4m(\sqrt{2m} + 2) + 2\sqrt{2m}} \\ &\quad + B + 2Cm + 3Dm^2 + 4Em^3. \end{aligned} \quad (8)$$

The missing gradient $\frac{d\mu_{\text{NaOH}}}{dz}$ in Eq. 7 can be derived from Eqs. 5 and 6 resulting in

$$\begin{aligned} \frac{d\mu_{\text{NaOH}}}{dz} &= \frac{RT M_{\text{H}_2\text{O}}}{\rho_{\text{NaOH}}} \cdot \frac{m M_{\text{NaOH}} + 1}{2m M_{\text{H}_2\text{O}} + 1} \\ &\quad \times \left(\frac{N_{\text{H}_2\text{O}}^l}{D_{\text{Na}^+, \text{H}_2\text{O}, n}^{\text{eff}}} + \frac{N_{\text{H}_2\text{O}}^l - \frac{N_{\text{OH}^-}}{m M_{\text{H}_2\text{O}}}}{D_{\text{OH}^-, \text{H}_2\text{O}, n}^{\text{eff}}} \right), \end{aligned} \quad (9)$$

where ρ_{NaOH} is the density of the sodium hydroxide solution. This equation is valid for a Na^+ flux of zero (see Sect. 3.4).

3.4 Material balances

From the overall integral material balances, it follows that the fluxes of nitrogen and sodium ions are zero, because they do not participate in the reaction (Eq. 1).

$$N_{\text{N}_2} = 0 \quad (10)$$

$$N_{\text{Na}^+} = 0$$

Water on the other hand is able to flow from the gas chamber to the electrolyte or vice versa, even in the absence of reaction, depending on the conditions in the gas chamber.

In Fig. 3, it can be seen that water in the reaction layer can either flow in the gas phase ($N_{\text{H}_2\text{O}}^g$) or in the electrolyte phase ($N_{\text{H}_2\text{O}}^l$). The sum of these two fluxes gives the total flow of water

$$N_{\text{H}_2\text{O}} = N_{\text{H}_2\text{O}}^g + N_{\text{H}_2\text{O}}^l. \quad (11)$$

If the electrochemical reaction takes place the flux of oxygen at the beginning of the reaction layer is coupled to the flux of OH^- ions at the end of the reaction layer according to the stoichiometry of the reaction.

$$N_{\text{OH}^-}(z = z_t) = 4N_{\text{O}_2}(z = 0) \quad (12)$$

For the water consumed by the reaction, we obtain

$$N_{\text{H}_2\text{O}}(z = 0) - N_{\text{H}_2\text{O}}(z = z_t) = 2N_{\text{O}_2}(z = 0). \quad (13)$$

The flux of oxygen can be calculated with Faraday's law

$$j_e(z = 0) = -4FN_{\text{O}_2}(z = 0), \quad (14)$$

where j_e is the current density in the solid electrode. The integral material balances inside the reaction layer yield

$$N_{\text{OH}^-}(z) = N_{\text{OH}^-}(z_t) - 4N_{\text{O}_2}(z) \quad (15)$$

$$N_{\text{H}_2\text{O}}(z) = N_{\text{H}_2\text{O}}(z_t) + 2N_{\text{O}_2}(z) \quad (16)$$

$$j_e(z) = -4FN_{\text{O}_2}(z). \quad (17)$$

As no reaction is taking place in the diffusion layer and the boundary layer, the fluxes of the gaseous species are equal to the fluxes at the beginning of the reaction layer

$$N_i^g(z = 0) = N_i(z') = N_i(z''). \quad (18)$$

Equations 12–18 allow for the calculation of all fluxes if the flux of oxygen is known at each position in the reaction layer. This missing quantity can be calculated with the differential material balance

$$r = -\frac{dN_{\text{O}_2}}{dz}, \quad (19)$$

where r is the reaction rate of oxygen.

With the equations above the partial pressures and concentration profiles in the agglomerates can be calculated along the z -axis (Fig. 4a).

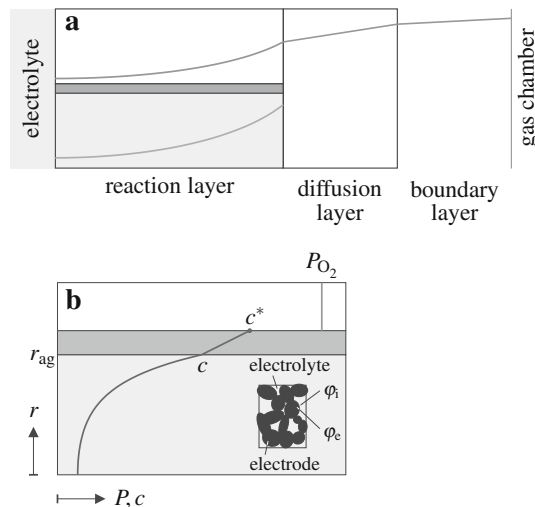


Fig. 4 Schematic of partial pressure and concentration profiles in the various regions

3.5 Diffusion and reaction of oxygen in the electrolyte

Before the electrochemical reaction takes place, oxygen must dissolve in the film which is surrounding the agglomerates. Henry's law is used to describe the equilibrium between the gas phase and the film (assumption 10)

$$c^* = \frac{P_{\text{O}_2}}{H}, \quad (20)$$

where c^* is the concentration of oxygen in the outer film and H the (inverse) Henry constant (dot in Fig. 4b). The oxygen then diffuses through the film followed by coupled diffusion and reaction inside the agglomerates. In steady state, the diffusion flux through the film has to be equal to the reaction rate in the agglomerates. The diffusion flux through the film can be described by

$$r = \frac{D_{\text{O}_2}^l}{\delta_{\text{tf}}} (c^* - c) S_{\text{tf}} \quad (21)$$

with the thickness of the film δ_{tf} , the concentration difference between the outermost and innermost point of the film $c^* - c$ (straight line in Fig. 4b) and the specific surface area of the thin film per total reaction layer volume S_{tf} . The specific surface area of the thin film related to the total volume of the reaction layer can be calculated with

$$S_{\text{tf}} = \frac{2}{r_{\text{ag}}} (1 - \varepsilon_t). \quad (22)$$

The coupled diffusion and reaction of oxygen in the agglomerates can be described analogous to the well-known phenomena taking place in a porous catalyst particle [19]

$$r = k_c c \eta_{\text{eff}} (1 - \varepsilon_t), \quad (23)$$

where k_c is the reaction rate constant, c the concentration of oxygen at the outermost point of the agglomerate and η_{eff} the effectiveness factor (cf. curve in Fig. 4b). The effectiveness factor can be calculated with the aid of the Thiele modulus γ

$$\eta_{\text{eff}} = \frac{\tanh(\gamma)}{\gamma} \quad (24)$$

where

$$\gamma = L \sqrt{\frac{k_c}{D_{O_2}^{\text{eff},l}}} \quad (25)$$

and L the characteristic length which is

$$L = r_{\text{ag}}/2 \quad (26)$$

for the considered cylindrical geometry.

With the maximum oxygen concentration c and the effectiveness factor η_{eff} , one can also calculate an effective concentration inside the agglomerate

$$c^{\text{eff}} = c \eta_{\text{eff}}. \quad (27)$$

3.6 Electrochemical reaction, potential and current density distribution

The electrochemical reaction is described with the Tafel equation assuming that there is a change in the rate determining step (assumption 13)

$$j_{\text{tf}} = \begin{cases} A_1 c \cdot 10^{\frac{\Delta\varphi}{T_{s1}}} & \text{for } \eta \leq E_{\text{change}}, \\ A_2 c \cdot 10^{\frac{\Delta\varphi}{T_{s2}}} & \text{for } \eta > E_{\text{change}} \end{cases} \quad (28)$$

where j_{tf} is the current density transferred per area of thin film, which is connected with the reaction rate by

$$r = \frac{j_{\text{tf}}}{4F} S_{\text{tf}}. \quad (29)$$

A_1 and A_2 are constants describing the exchange current density, T_{s1} and T_{s2} the corresponding Tafel slopes, η the overpotential, and $\Delta\varphi$ the potential difference between the solid electrode and the electrolyte in the porous electrode

$$\Delta\varphi = \varphi_e - \varphi_i. \quad (30)$$

The potential distribution inside the solid electrode φ_e and the electrolyte φ_i can be calculated by Ohm's law

$$\frac{d\varphi_e}{dz} = -\frac{j_e}{\kappa_e} \quad (31)$$

$$\frac{d\varphi_i}{dz} = -\frac{j_i}{\kappa_i^{\text{eff}}} \quad (32)$$

with the conductivity of the solid electrode κ_e and the effective conductivity of the electrolyte κ_i^{eff} inside the

pores of the agglomerate, which can be calculated from the conductivity of the free electrolyte κ_i

$$\kappa_i^{\text{eff}} = \kappa_i \frac{\varepsilon_n}{\tau_n} (1 - \varepsilon_t) \quad (33)$$

with the porosity of the agglomerates

$$\varepsilon_n = \frac{\varepsilon_s - \varepsilon_t}{1 - \varepsilon_t}. \quad (34)$$

The current density distribution of the electrode was already given in Eq. 17 and the current density distribution of the electrolyte can be easily calculated with

$$j = j_e + j_i \quad (35)$$

where j is the current density externally applied to the ODC.

The overpotential η is defined as

$$\eta = [\varphi_e(0) - \varphi_i(z_t)] - E^\circ \quad (36)$$

because the bracketed potential difference can be measured experimentally. E° is the standard potential at $T = 80$ °C and a partial pressure of oxygen in the gas chamber of 1 bar which is equal to 0.218 V [25].

3.7 Diffusion coefficients

The Knudsen diffusion coefficients are calculated with

$$D_{i,\text{K},x} = \frac{2}{3} r_x \sqrt{\frac{8RT}{\pi M_i}} \quad \text{with } x = s, t \quad (37)$$

based on the kinetic gas theory. All required effective diffusion coefficients are calculated by multiplying the free binary diffusion coefficients with the porosity–tortuosity factor. The same holds for the calculation of the effective Knudsen diffusion coefficients and the effective diffusion coefficient of oxygen in the agglomerate.

$$D_x^{\text{eff}} = \frac{\varepsilon_x}{\tau_x} D_x \quad \text{with } x = s, t, n \quad (38)$$

$$D_{O_2}^{\text{eff},l} = \frac{\varepsilon_n}{\tau_n} D_{O_2}^l \quad (39)$$

3.8 Model implementation and boundary conditions

The model was build in Aspen Custom Modeler (ACM) using all shown equations above except Eqs. 1, 5, and 6 which were only numbered for referencing purposes. Equation 2 was used for oxygen and water vapor while the nitrogen partial pressure was calculated as difference to the total pressure

$$P_{\text{T,b}} = \sum P_i. \quad (40)$$

The total pressure in the boundary layer equals the total pressure in the gas chamber due to assumption 2

$$P_{T,b} = P_{T,g}. \quad (41)$$

The boundary conditions for these two differential equations are that the “inlet” partial pressures are equal to the partial pressures in the gas chamber

$$P_i(z'' = 0) = P_{i,g} \quad \text{with} \quad i = \text{O}_2, \text{H}_2\text{O}. \quad (42)$$

The same principle was used for the gas diffusion layer and the gas channels in the reaction layer (Eqs. 3, 4) except that the “inlet” partial pressures of the domains are the “outlet” partial pressures of the previous domains, i.e.,

$$P_{i,s}(z' = 0) = P_{i,b}(z'' = z_b) \quad \text{with} \quad i = \text{O}_2, \text{H}_2\text{O} \quad (43)$$

$$P_{i,t}(z = 0) = P_{i,s}(z' = z_s) \quad \text{with} \quad i = \text{O}_2, \text{H}_2\text{O}. \quad (44)$$

The boundary condition for Eq. 7 is

$$m(z_t) = 11.25 \text{ mol kg}^{-1} \quad (45)$$

which is the concentration of the considered electrolyte. After calculation of the concentration profiles in the electrolyte, the partial pressure of water in the gas channels of the reaction layer is immediately known due to assumption 11

$$P_{\text{H}_2\text{O}} = P_m \quad (46)$$

with P_m as the saturation partial pressure of water above the aqueous sodium hydroxide solution. As the partial pressure of water in the gas chamber is also known, the flux of water vapor in the gas diffusion layer and the boundary layer can be calculated. However, since the flux of oxygen is given by Faraday’s law (Eqs. 14, 18), conflicts arise if the case of a gas phase containing only oxygen without nitrogen is considered. Therefore, we have chosen to always assume that a certain amount of nitrogen is present in the system (for further details see [26]). To calculate the case of pure oxygen in the gas chamber, we use a partial pressure of nitrogen of 0.1 bar which is also added to the total pressure of the system.

In order to achieve that no (gaseous) oxygen is exchanged with the electrolyte at the end of the reaction layer, the following boundary condition for Eq. 19 is used

$$N_{\text{O}_2}(z_t) = 0. \quad (47)$$

The same applies to water vapor at that boundary

$$N_{\text{H}_2\text{O}}^g(z_t) = 0 \quad (48)$$

and for liquid water at the boundary between reaction layer and gas diffusion layer

$$N_{\text{H}_2\text{O}}^l(z = 0) = 0. \quad (49)$$

The remaining boundary conditions concern Ohm’s laws. For Eq. 31, the current density in the solid electrode

at the beginning of the reaction layer equals the externally applied current density

$$j_e(z = 0) = j \quad (50)$$

and for Eq. 32, we have chosen to set

$$\varphi_i(z = 0) = 0, \quad (51)$$

because the two potentials φ_e and φ_i cannot be observed independently.

4 Determination of experimental and model parameters

The electrode used for the measurement of overpotentials was prepared by a spray method that will be described elsewhere. It had a thickness of 300 μm and consisted of a mixture of 97 wt% silver and 3 wt% PTFE. The oxygen reduction was carried out in a half-cell from Gaskatel GmbH, Germany, under galvanostatic conditions at 80 °C and ambient pressure with controlled flows of NaOH and mixtures of oxygen and nitrogen (saturated with water vapor at ambient temperature) on both sides of the electrode. The potential as a function of current was measured with the aid of a Luggin capillary placed directly on the surface of the catholyte side of the ODC. A HydroFlex electrode from Gaskatel GmbH, Germany, was used as reference electrode. The measured electronic conductivity of the electrode was found to be $\geq 10^5 \text{ S m}^{-1}$. The experimental and model parameters required for the simulations are listed in Tables 1 and 2.

The current density was calculated through dividing the applied current by the geometrical surface of the electrode exposed to the electrolyte. The measured potential (vs. RHE) of the electrode was first corrected to NHE and then the standard potential of the oxygen reduction reaction (ORR) was subtracted to obtain the overpotential.

5 Results and discussion

The developed ODC model allows for the simulation of overpotentials as a function of current density for various operating conditions. Before attempting to fit the model parameters to the measured overpotentials, a numerical study was performed to identify the most significant parameters. In agreement with [6], it was found that the diffusion of oxygen in the gas phase is only limiting when the radii of the gas pores are very small. For the pore radii in the electrode (Table 1) the diffusion of oxygen is never limiting even at extremely high current densities. The most relevant phenomena are thus the electrochemical reaction and the diffusion of oxygen in the liquid electrolyte.

Table 1 List of constant model parameters for standard case (100% O₂)

Name	Symbol	Unit	Value	Remarks
Boundary layer in gas chamber				
Thickness	z_b	m	15×10^{-3}	Own estimate
Gas diffusion layer				
Averaged radius	r_s	m	5.0×10^{-7}	Own estimate
Porosity	ε_s	Dimensionless	0.40	Own estimate
Tortuosity	τ_s	Dimensionless	3	Own estimate
Reaction layer				
Averaged radius for the gas channels	r_t	m	2.5×10^{-7}	Own estimate
Tortuosity for the gas channels	τ_t	Dimensionless	1	Assumption 5
Tortuosity of the agglomerates	τ_n	Dimensionless	3	Own estimate
Operating conditions				
O ₂ partial pressure in gas chamber	$P_{O_2,g}$	Pa	1.0×10^5	
H ₂ O partial pressure in gas chamber	$P_{H_2O,g}$	Pa	0.0234×10^5	Saturated at 20 °C
N ₂ partial pressure in gas chamber	$P_{N_2,g}$	Pa	0.1×10^5	See text
NaOH molality in catholyte	m	mol kg ⁻¹	11.25	
Temperature	T	K	353.15	
Electrochemical reaction				
Equilibrium potential	E°	V	0.214	[24, 25]
(Fixed) property data				
Electronic conductivity of the electrode	κ_e	S m ⁻¹	1×10^5	See text
Ionic conductivity of the electrolyte	κ_i	S m ⁻¹	120	[27] Figure H10]
(Inverse) Henry constant	H	Pa m ³ mol ⁻¹	8.55×10^6	[28]
O ₂ diffusion coefficient in the electrolyte	$D_{O_2}^l$	m ² s ⁻¹	2.54×10^{-9}	[28]

Table 2 Property data dependent on temperature or other parameters (m , r)

Name	Symbol	Unit	Remarks
Diffusion coefficients			
Binary gas diffusion coefficients	D_{ij}^g	m ² s ⁻¹	[29] ^a
Knudsen diffusion coefficients	$D_{i,K}$	m ² s ⁻¹	Eq. 37
Binary liquid diffusion coefficients	D_{ij}^l	m ² s ⁻¹	[22] ^b
Catholyte data			
Mean molal activity coefficient of NaOH in aqueous NaOH solution	γ_\pm	Dimensionless	[24] ^c
Vapor pressure of H ₂ O in aqueous NaOH solution	P_m	Pa	[24] ^c
Activity of H ₂ O in aqueous NaOH solution	a_{H_2O}	Dimensionless	[24] ^c
Saturation vapor pressure of pure H ₂ O	$P_{H_2O}^{sat}$	Pa	[30]
Density of aqueous NaOH solution	ρ_{NaOH}	kg m ⁻³	[31]

^a With corrected equation 11-3.1

^b Calculated for KOH with viscosity data of NaOH from [31], because NaOH data are not available

^c 0.1–17 mol kg⁻¹, 0–70 °C → data extrapolated

We started with the description of the overpotential in the region of current densities below 0.5 kA m⁻², where diffusion resistances are relatively low for the case of 100% oxygen. First, it was attempted to describe the measured results based on a single Tafel equation (light gray lines in Fig. 5a). Note that the gray area where the Tafel equation is assumed to be invalid refers to potentials

up to $5RT/4F = 38$ mV. With a single Tafel equation, however, it was not possible to predict the relatively high overpotentials at higher current densities with severe diffusion limitations as indicated by the thin gray line in Fig. 5b. Therefore, we introduced a second Tafel equation in the region of higher potentials (>0.155 V) with about twice the slope of the low potential curve. With this

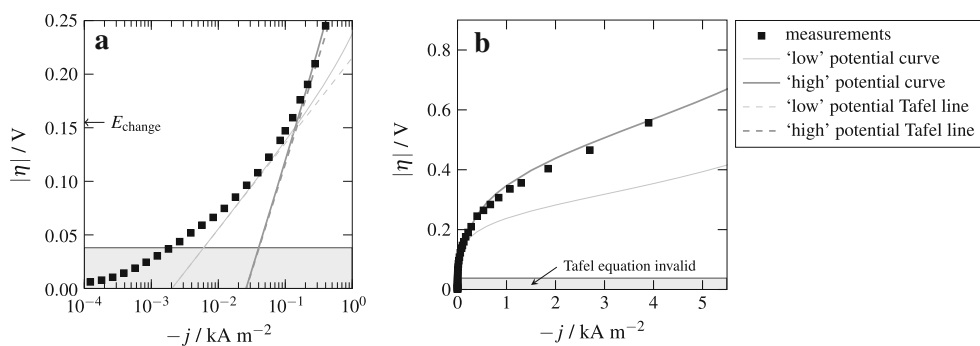


Fig. 5 Comparison between simulation results and measurements for 100% O₂

extension it was possible to describe the overpotentials in both the kinetic regime and for industrially relevant current densities (Fig. 5). The differences between the broken lines in Fig. 5a, that denote the Tafel slopes, and the solid lines, which were calculated with the full model, reveal that the influence of mass transfer resistances already becomes relevant at current densities as low as 0.1 kA m⁻² (see also discussion of Fig. 8).

A possible reason for the apparent change in the Tafel slope could be a change of the adsorption isotherms. This was found during the ORR on platinum catalysts where the charge transfer step was rate determining in both potential regions and the observed difference in the Tafel slopes arose solely from different adsorption isotherms of the intermediate species in the both regions [32, 33]. Another explanation for this effect could be the porous nature of the ODC itself. With a statistical model, Soderberg et al. [34] have shown that strongly different electronic and ionic conductivities may lead to an apparent doubling of the Tafel slope even in the absence of mass transfer resistances.

The diagrams in Fig. 6 reveal that the developed model also allows for the description of measurements obtained at different oxygen concentrations with quite good accuracy. The Tafel curves depicted in Fig. 6a are shifted to lower

current densities according to the lower equilibrium oxygen concentration in the electrolyte. The calculated limiting current densities for diluted gas mixtures with 30 to 50% O₂ are around 2 and 3.5 kA m⁻², respectively. However, these predicted limiting current densities cannot be measured, because the reaction will switch from the ORR to the hydrogen evolution reaction if the potential for this reaction is lower than that of the ORR. Nevertheless, the results clearly show that industrially relevant current densities of 4 kA m⁻² or higher can only be reached with oxygen concentrations of or close to 100%.

Some interesting further simulation results are summarized in Fig. 7. Figure 7 shows the fluxes of all the species in the reaction layer for an externally applied current density of 4 kA m⁻² and 100% oxygen. As described earlier the flux of oxygen can be calculated by Faradays law and has to decrease to zero at the end of the reaction layer. In contrast, the flux of the hydroxide ions rises from 0 to 4 times the flux of oxygen at z = 0, and the difference of the fluxes of the total water N_{H₂O} between z = 0 and z = z_t has to be twice the flux of oxygen at the beginning of the reaction layer (Eq. 13). The net flux of water toward the gas chamber is caused by the lower partial pressure of water in the gas chamber compared to that in the reaction layer. The consequence of the rising flux of OH⁻ ions

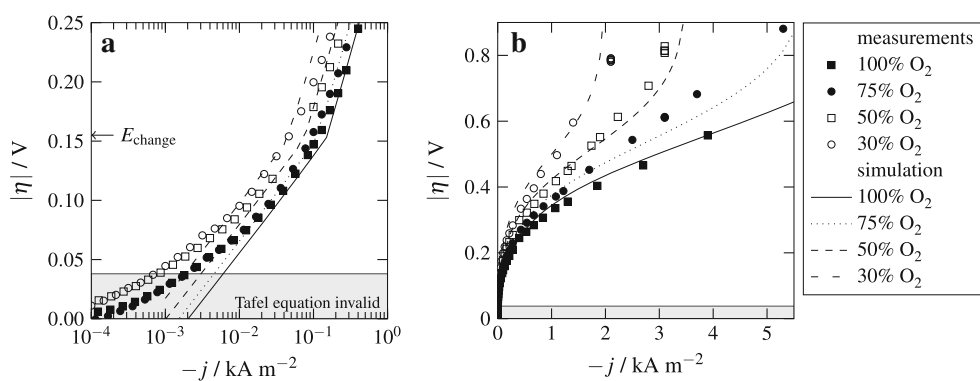
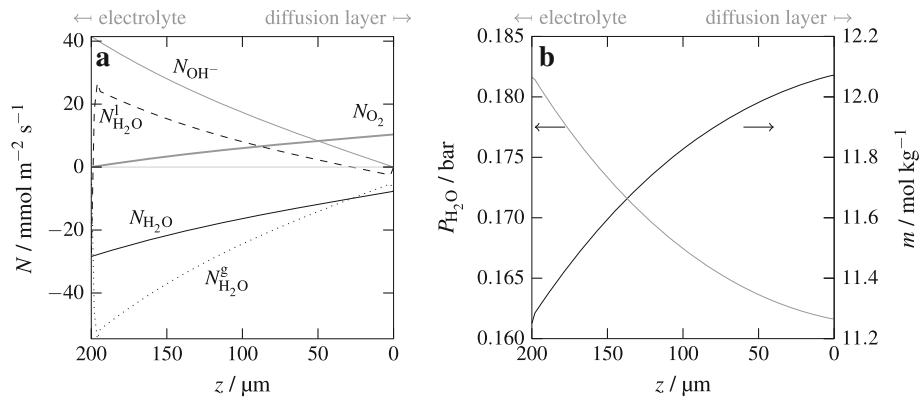


Fig. 6 Dependence of overvoltage on current density for different oxygen concentrations

Fig. 7 **a** Fluxes of species, molality of NaOH and **b** water partial pressure distribution in the reaction layer



toward the electrolyte is that the molality of the sodium hydroxide solution is decreasing which also causes a rise of the partial pressure of water around the agglomerates (Fig. 7b). This results in a negative flux of the water vapor, and to fulfill Eq. 11 the flux of liquid water is positive in most cases. The sharp edges at the ends of the gas and liquid fluxes of water result from the conditions given in Eqs. 48 and 49 and the fact that no kinetic limitation for the phase transfer of water was taken into account.

It is also very instructive to discuss the calculated oxygen distribution inside the agglomerates and the surrounding film as shown for three different current densities

in Fig. 8. The spatial distribution of oxygen concentration for an isothermal reaction–diffusion system with first order kinetics can be calculated with [35]

$$c(r, z) = c(r_{\text{ag}}, z) \frac{\cosh\left(\frac{r}{r_{\text{ag}}} \gamma(z)\right)}{\cosh(\gamma(z))}. \quad (52)$$

For simplicity, only results in the middle of the reaction layer are shown. Already for a relatively low current density of 0.5 kA m^{-2} the oxygen concentration decreases to almost zero in a thin outer layer of the agglomerate. Thus more than 90% of the agglomerates do not participate

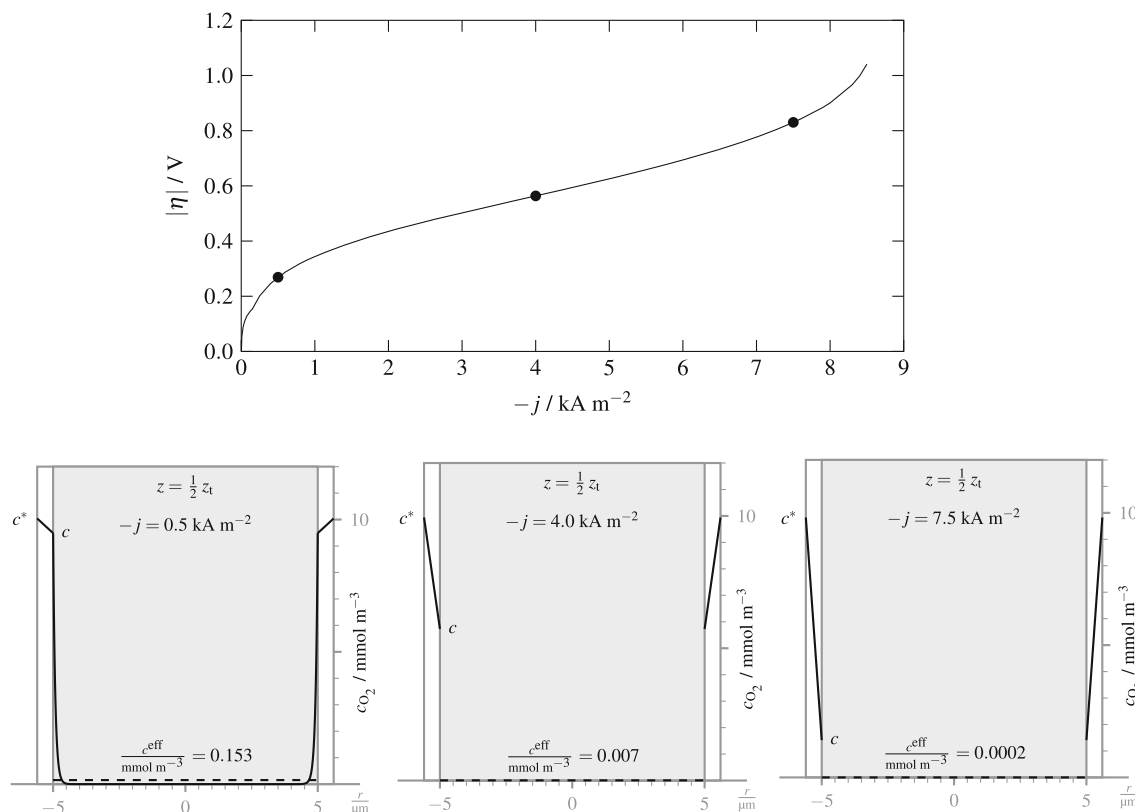


Fig. 8 Distribution of oxygen concentration in film and agglomerate at different current densities for 100% O₂, thin film magnified by a factor of 10

Table 3 Adjusted model parameters to fit measured data

Name	Symbol	Unit	Value	Remarks
Gas diffusion layer				
Thickness	z_s	m	1.0×10^{-4}	a
Reaction layer				
Thickness	z_t	m	2.0×10^{-4}	a
Porosity	ε_t	Dimensionless	0.32	
Averaged radius for the agglomerates	r_{ag}	m	5.0×10^{-6}	
Thickness of the film	δ_{tf}	m	6.0×10^{-8}	
Electrochemical reaction				
Low potential region				
Constant	A_1	$A \text{ m mol}^{-1}$	0.007	
Tafel slope	T_{s1}	$V \text{ decade}^{-1}$	0.08	
High potential region				
Constant	A_2	$A \text{ m mol}^{-1}$	4.0	
Tafel slope	T_{s2}	$V \text{ decade}^{-1}$	0.20	

^a Sum of z_s and z_t assumed to be equal to total thickness of electrode

in the reaction and the effective concentration c^{eff} is around 60 times lower than the maximum concentration in the agglomerate c . This value is still similar to the maximum concentration in the film c^* indicating no significant resistance due to film diffusion.

The supply of oxygen to the active sites of the silver electrocatalyst is even worse for an industrial relevant current density of 4 kA m^{-2} where one already can see a significant influence of the film surrounding the agglomerate. The oxygen concentration reaching the agglomerate drops by about 40% and the concentration inside the agglomerate falls so rapidly that it cannot be depicted anymore. Although the effective concentration in the agglomerates is now around 1500 times lower than the equilibrium value, the electrode is still working properly below the limiting current density, however, at the expense of an overpotential of more than 500 mV. At a current density of 7.5 kA m^{-2} the electrode reaches the border of the mass transfer limitation with the concentration at the end of the liquid film being hardly more than 10% of the maximum value.

The kinetic parameters for the electrochemical reaction could be determined with quite good accuracy (cf. Fig. 5). Nevertheless, future measurements on non-porous electrodes made from the same silver catalyst should help to verify the electrokinetics independently. The remaining model parameters that had to be adjusted were the thickness and porosity of the reaction layer as well as agglomerate radius and thickness of the surrounding film (Table 3). The film thickness for which a very low value of 60 nm was obtained can be determined relatively independently from the onset of mass transfer limitation at a given oxygen concentration in the gas phase. The other

three geometric parameters, however, can only be determined simultaneously and different parameter sets allow for the description of the measured overpotentials with similar accuracy. To determine these parameters more precisely, it would be highly desirable to measure the distribution of the liquid electrolyte in the porous electrode under reaction conditions. This is, however, a quite difficult task for future investigations given the estimated average agglomerate radius in the range of only 5 μm .

6 Conclusion

We have presented a model for the calculation of the overpotential during oxygen reduction on a silver-based ODC in a wide range of current densities. With this model it is possible to study the influence of reaction conditions such as temperature, electrolyte concentration, and gas composition on the electrode performance. It is also evident that the electrode can be operated at high current densities although the by far larger parts of the agglomerates do not contribute to the reaction. Thus the electrochemical reaction in the *working* parts of the electrode is extremely fast. Therefore, an improved electrode should consist of very small catalyst particles, which are only wetted by a film of similar size, provided that the flow of hydroxide ions does not become the rate determining step. The size of the gas channels is of lesser importance as diffusion in the gas phase is orders of magnitude faster than in the electrolyte. Such an improved geometric electrode design would result in high surface areas between gas phase and electrolyte as well as between electrolyte and solid catalyst.

Acknowledgments The authors would like to thank Dr. Norbert Wagner from DLR Stuttgart for measuring the electronic conductivity of the electrode and providing the SEM micrographs. Gregor Polcyn and Prof. Jakob Jörissen from TU Dortmund are also kindly acknowledged for the half-cell measurements. This research was funded by the German ministry of education and research (BMBF) under the klimazwei programme.

References

1. World Chlorine Council – What is the WCC? <http://www.worldchlorine.org/about/index.html>. Accessed 1 Dec 2010
2. Moussallem I, Jörissen J, Kunz U, Pinnow S, Turek T (2008) *J Appl Electrochem* 38(9):1177. doi:[10.1007/s10800-008-9556-9](https://doi.org/10.1007/s10800-008-9556-9)
3. Moussallem I, Pinnow S, Turek T (2009) *Chem Ing Tech* 81(4):489. doi:[10.1002/cite.200800172](https://doi.org/10.1002/cite.200800172)
4. Nachrichten – Bayer Sustainable Development Report 2009 <http://www.sustainability2009.bayer.com/en/news-detail.aspx?newsid=1835>. Accessed 1 Dec 2010
5. Wang XL, Koda S (1997) *Denki Kagaku* 65(12):1002
6. Wang XL, Koda S (1997) *Denki Kagaku* 65(12):1014
7. Bidault F, Brett DJL, Middleton PH, Brandon NP (2009) *J Power Sourc* 187(1):39. doi:[10.1016/j.jpowsour.2008.10.106](https://doi.org/10.1016/j.jpowsour.2008.10.106)
8. Will FG (1963) *J Electrochim Soc* 110(2):152. doi:[10.1149/1.2425693](https://doi.org/10.1149/1.2425693)
9. Austin LG, Ariet M, Walker RD, Wood GB, Comyn RH (1965) *Ind Eng Chem Fund* 4(3):321. doi:[10.1021/i160015a015](https://doi.org/10.1021/i160015a015)
10. Srinivasan S, Hurwitz HD (1967) *Electrochim Acta* 12(5):495. doi:[10.1016/0013-4686\(67\)80019-7](https://doi.org/10.1016/0013-4686(67)80019-7)
11. Srinivasan S, Hurwitz HD, Bockris JOM (1967) *J Chem Phys* 46(8):3108. doi:[10.1063/1.1841182](https://doi.org/10.1063/1.1841182)
12. Markin VS (1963) *Russ Chem Bull* 12(9):1551. doi:[10.1007/BF00844119](https://doi.org/10.1007/BF00844119)
13. Burshtein RC, Markin VS, Pshenichnikov AG, Chismadgev VA, Chirkov YG (1964) *Electrochim Acta* 9(6):773. doi:[10.1016/0013-4686\(64\)80064-5](https://doi.org/10.1016/0013-4686(64)80064-5)
14. Grens EA II, Tobias CW (1965) *Electrochim Acta* 10(8):761. doi:[10.1016/0013-4686\(65\)80041-X](https://doi.org/10.1016/0013-4686(65)80041-X)
15. Grens EA II (1970) *Electrochim Acta* 15(6):1047. doi:[10.1016/0013-4686\(70\)80044-5](https://doi.org/10.1016/0013-4686(70)80044-5)
16. Giner J, Hunter C (1969) *J Electrochim Soc* 116(8):1124. doi:[10.1149/1.2412232](https://doi.org/10.1149/1.2412232)
17. Cutlip MB (1975) *Electrochim Acta* 20(10):767. doi:[10.1016/0013-4686\(75\)85013-4](https://doi.org/10.1016/0013-4686(75)85013-4)
18. Iczkowski RP, Cutlip MB (1980) *J Electrochim Soc* 127(7):1433. doi:[10.1149/1.2129925](https://doi.org/10.1149/1.2129925)
19. Björnbom P (1987) *Electrochim Acta* 32(1):115. doi:[10.1016/0013-4686\(87\)87018-4](https://doi.org/10.1016/0013-4686(87)87018-4)
20. Yang SC, Cutlip MB, Stonehart P (1990) *Electrochim Acta* 35(5):869. doi:[10.1016/0013-4686\(90\)90083-C](https://doi.org/10.1016/0013-4686(90)90083-C)
21. Yang SC, Björnbom P (1992) *Electrochimica Acta* 37(10):1831. doi:[10.1016/0013-4686\(92\)85087-2](https://doi.org/10.1016/0013-4686(92)85087-2)
22. Newman J, Bennion D, Tobias CW (1965) *Ber Bunsenges* 69:608
23. Newman J (1967) *Adv Electrochim Electrochem Eng* 5:87
24. Åkerlöf G, Kegelis G (1940) *J Am Chem Soc* 62(3):620. doi:[10.1021/ja01860a057](https://doi.org/10.1021/ja01860a057)
25. Bratsch SG (1989) *J Phys Chem Rev Data* 18(1):1
26. Pinnow S (2011) Modellierung von Sauerstoffverzehrkathoden für die Chloralkali-Elektrolyse. Ph.D. thesis, TU Clausthal
27. O'Brien TF, Bommaraju TV, Hine F (2005) *Handbook of chlor-alkali technology*, volume V: corrosion, environmental issues, and future developments. Springer Science+Business Media Inc., New York
28. Chatenet M, Aurousseau M, Durand R (2000) *Ind Eng Chem Res* 39(8):3083. doi:[10.1021/ie000044g](https://doi.org/10.1021/ie000044g)
29. Poling BE, Prausnitz JM, O'Connell JP (2000) *The Properties of Gases and Liquids*, 5th edn. McGraw-Hill, New York
30. Wagner W, Prüß A (2002) *J Phys Chem Rev Data* 31(2):387. doi:[10.1063/1.1461829](https://doi.org/10.1063/1.1461829)
31. Olsson J, Jernqvist Å, Aly G (1997) *Int J Thermophys* 18(3):779. doi:[10.1007/BF02575133](https://doi.org/10.1007/BF02575133)
32. Sepa DB, Vojnovic MV, Vracar LM, Damjanovic A (1986) *Electrochim Acta* 31(1):91. doi:[10.1016/0013-4686\(86\)80067-6](https://doi.org/10.1016/0013-4686(86)80067-6)
33. Sepa DB, Vojnovic MV, Vracar LM, Damjanovic A (1986) *Electrochim Acta* 31(1):97. doi:[10.1016/0013-4686\(86\)80068-8](https://doi.org/10.1016/0013-4686(86)80068-8)
34. Soderberg JN, Co AC, Sirk AHC, Birss VI (2006) *J Phys Chem B* 110(21):10401. doi:[10.1021/jp060372f](https://doi.org/10.1021/jp060372f)
35. Kunz U, Peuker U, Turek T, Estenfelder M (2006) In: Bröckel U, Meier W, Wagner G (eds) *Product Design and Engineering: Best Practices*, vol 2. Wiley-VCH, Weinheim, pp 485–521